Journal of Materials Chemistry A

Accepted Manuscript

ROYAL SOCIETY OF CHEMISTRY

www.rsc.org/materialsA

Journal of Materials Chemistry A

Dynamic Article Links ►

Cite this: DOI: 10.1039/c0xx00000x

ARTICLE TYPE

www.rsc.org/xxxxxx

A "H_2O donating/methanol accepting" platform for preparation of highly selective Nafion-based proton exchange membranes†

Kai Feng, Beibei Tang* and Peiyi Wu*

Received (in XXX, XXX) Xth XXXXXXXXX 20XX, Accepted Xth XXXXXXXXX 20XX

DOI: 10.1039/b000000x

For proton exchange membrane (PEM), the ratio of its proton conductivity to its fuel permeability usually defines the membrane selectivity. Generally, highly selective PEM is preferred in the applications of direct methanol fuel cell. Herein, sulfonated SiO_2@polystyrene core-shell (SiO_2@sPS) nanoparticles were synthesized and then imbedded into Nafion membrane by a blending-casting method. SiO_2@sPS possesses strong interactions with Nafion polymer, which benefits its dispersion in the membrane matrix. The as-prepared SiO_2@sPS+Nafion composite PEM presents a large increase in proton conductivity owing to the introduction of additional -SO_3H groups and hence optimized channels for proton transport. Meanwhile, reduced methanol crossover was also observed on the SiO_2@sPS+Nafion composite PEM because of the formation of obstructed transport channels for bulk methanol. Besides, deep investigation on further enhancement of membrane performance was conducted by etching the SiO_2 core and hence forming well-dispersed uniform hollow spheres inside the membrane matrix. The intact hollow sulfonated PS spheres (h-sPS) acted as water reservoirs which could gradually release water to hydrate the membrane in turn under high-temperature and low-humidity conditions. Therefore, compared to the SiO_2@sPS+Nafion membrane, the h-sPS+Nafion one presented further increased proton conductivity at 100 ^oC under 40%RH. Meanwhile, h-sPS further suppressed the methanol penetration by blocking it inside the hollow spheres. Herein, a "H_2O donating/methanol accepting" mechanism was proposed for the first time, providing a promising platform to alleviate critical disadvantages of Nafion membranes and thereby fabricate highly selective Nafion-based PEMs.

1 Introduction

Proton exchange membrane fuel cell (PEMFC) provides a promising alternative to the conventional internal combustion engines owing to its environmental friendliness and high energy conversion efficiency.[1,2] It triggers extensive efforts with a view to driving the traditional society dependent on fossil fuels to move into a new world powered by clean energy technologies. Among PEMFCs, direct methanol fuel cell (DMFC) outstands by virtue of its distinctive advantages, such as high volumetric and specific energy densities, moderate temperature operation, no requirement of a fuel reformer, low emission and long lifetime. Besides, the fuel storage problems, typical of hydrogen fed fuel cell, do not concern DMFC, because the liquid nature of methanol endows great convenience in the transportation and storage of fuel upon DMFC. It is very attractive especially when the environmental and economic concerns become stressing in modern society. DMFC may claim a niche in the market of mobile electrical power generators.

DMFC employs a proton exchange membrane (PEM) to separate methanol from oxidant and simultaneously conduct protons from the anode to the cathode to fulfill the conversion of chemical energy into electrical energy. Therefore, PEM, acting as a vital building component of DMFC, plays a pivotal role in the DMFC performance. Perfluorosulfonated polymers e.g. Nafion are the current state-of-the-art commercial PEMs.[1] Nafion possesses a polytetrafluoroethylene backbone with short perfluoroether side chains bearing terminal -SO_3H groups. The hydrophobic regions bestow excellent thermo-mechanical stability and chemical resistivity upon Nafion membranes, while the hydrophilic domains form well-interconnected ionic channels which make high proton conductivity possible. All of these properties are requisite for the applications in DMFC. Besides, DMFC operated under high temperature and low humidity is often desired in the consideration of catalyst poisoning, fuel efficiency as well as heat and water management.[3] However, the typical drawbacks of Nafion membranes, i.e. reduction of proton conductivity above 80 ^oC and extensive methanol crossover, are detrimental for their practical applications in DMFC. Generally, any methanol crossover will decrease the overall fuel efficiency and simultaneously reduce the cell voltage. An ideal PEM should exhibit high proton conductivity with parallel low methanol crossover. However, proton and methanol almost migrate via the

same channels consisting of hydrophilic ionic cluster domains through a Nafion membrane.[2,4-6] In most cases, reduction of methanol crossover is achieved at the expense of proton conductivity, or *vice versa*. Therefore, the current Nafion-based PEMs still perform below the desired real-world application requirements, and development of PEMs with enhanced transport properties e.g. high proton conductivity and low methanol permeability generates renewed research attention.

Serious efforts go to eliminate such a tradeoff relationship between proton conductivity and methanol permeability of PEMs to render them suitable for real-world DMFC applications, namely: 1) development of alternative polymeric PEMs whose ionic clusters possess a small percolation size of methanol permeation, such as sulfonated poly(ether ether ketone), poly(arylene ether sulfone) and their derivatives as well as blends;[7-10] 2) design of special membrane textures, like double-layered[11-13] and sandwich-like[14-16] structures via surface treatment, mainly focusing on suppressing the methanol crossover of Nafion-based PEMs; 3) modification of Nafion membranes by impregnating organic/inorganic materials into Nafion matrix; *et al.* Of particular research interests is the third approach because it is convenient, effective and sometimes low-cost. These employed materials include one-dimensional (1D) carbon nanotube[17] and TiO_2 nanotube[18], 2D graphene flake[19] and its derivatives[4], 3D SiO_2[20-23], ZrO_2[24], laponite[25,26], montmorillonite[27], zeolite[28] and aluminosilicate[29] particles as well as polymers[30-33]. Generally, they can enhance the water retention capability of Nafion-based composite PEMs owing to their hydrophilicity. Besides, sulfonating these imbedded materials can further enhance the membrane performance because the sulfonic acid groups help form better interconnected ionic channels inside the Nafion matrix by enlarging and/or reorganizing the ionic cluster domains. As a result, further increase in proton conductivity is observed on these composite PEMs. This enhancement is strengthened under high-temperature or low-humidity conditions when the hopping mechanism dominates the proton conduction of Nafion membranes. Sometimes, reduced methanol crossover is surprisingly found probably because of the increased zigzag of diffusion channels of bulk methanol.[2,4]

However, inorganic materials often suffer from poor compatibility with Nafion polymer, resulting in unsatisfactory dispersion of the inorganic components in Nafion membrane. Hence, non-selective gaps may emerge in the membrane matrix with negative influences on membrane performance.[34] Although attaching organic components e.g. polymers onto the surface of inorganic materials can effectively strengthen the interactions between the additives and the membrane matrix, it usually hides the distinctive benefits of the inorganic components themselves in a napkin.

In this study, a new platform was developed to prepare highly selective Nafion-based PEMs with the aid of sulfonated organic-inorganic hybrid materials, where the ratio of proton conductivity to methanol permeability defines the membrane selectivity. To be specific, first, sulfonated SiO_2@polystyrene core-shell (SiO_2@sPS) nanoparticles were synthesized and then imbedded into Nafion membrane through a traditional blending-casting method. The sulfonated polystyrene (sPS) shell strengthens the interactions between SiO_2@sPS and the Nafion matrix via 1) –SO_3H (SiO_2@sPS) --- –SO_3H (Nafion) hydrogen bonding interactions and 2) hydrophobic interactions between PS chains and Nafion backbones. Hence, SiO_2@sPS nanoparticles dispersed well in the Nafion membrane. Resultantly, a significant increase in the proton conductivity of the SiO_2@sPS+Nafion composite PEM was observed because of the introduction of additional -SO_3H groups and hence optimized ionic cluster channels for proton transport. Meanwhile, the SiO_2@sPS+Nafion composite PEM presented reduced methanol permeability probably due to the increased tortuosity of methanol transport channels. Second, to reveal the distinctive advantages of the inorganic component, a template method was further utilized by etching the SiO_2 core to *in situ* form well-dispersed hollow sPS (h-sPS) spheres inside the membrane matrix. It further enhanced the membrane selectivity owing to the following two advantages. One was that a large amount of free H_2O could be reserved in the h-sPS spheres.[3,35,36] It rendered the h-sPS+Nafion composite PEM a stable water environment, resulting in a slower reduction of its proton conductivity under high temperature and/or low humidity. Second, methanol might be impeded by being captured inside the h-sPS spheres.[35,36] Herein, a "H_2O donating/methanol accepting" mechanism was proposed for the first time, providing another promising approach to alleviate critical disadvantages of Nafion-based PEMs.

2 Experimental

2.1 Materials

Tetraethylorthosilicate (TEOS), [3-(methacryloyloxy)propyl]trimethoxysilane (MPS), N,N'-methylenebisacrylamide (BIS), potassium persulfate and dimethyl sulfoxide-d6 (D-DMSO) were purchased from Aladdin. Absolute ethanol, ammonia, styrene, 1,2-dichloroethane, acetic anhydride, concentrated sulphuric acid, dimethylformamide (DMF), H_2O_2 solution and HF solution were provided by Sinopharm Chemical Reagent Co., Ltd. Nafion solution (perfluorinated resin solution, 5 wt% in lower aliphatic alcohol and water mixture) was obtained from Sigma-Aldrich. All the other reagents were received from commercial suppliers and used as received unless otherwise stated.

2.2 Preparation of SiO_2

First, 20 mL TEOS was added into a mixture of 70 mL H_2O, 162.5 mL absolute ethanol and 17.5 mL ammonia. The system was vigorously stirred (400 rpm) at 30 ^oC for 1 h. Then, white SiO_2 powder was obtained by centrifugation. It was washed with ethanol for several times before being vacuum-dried at 70 ^oC. At last, 5.2 g SiO_2 was produced.

2.3 Preparation of "SiO_2@="

0.5 g as-prepared SiO_2 powder was dispersed homogeneously in 250 mL absolute ethanol by being sonicated for at least 4 h. Subsequently, 15 mL MPS was added into the SiO_2/ethanol dispersion. The system was vigorously stirred at 40 ^oC for 24 h. Then, white powder was obtained by centrifugation. Lastly, it was washed with absolute ethanol for several times before being vacuum-dried at 50 ^oC. The product, MPS-modified SiO_2, was marked as "SiO_2@=" in the following sections.

2.4 Preparation of SiO_2@PS

0.26 g as-prepared "SiO_2@=" powder was dispersed homogeneously in 25 mL H_2O by being sonicated for 25 min. Then, N_2 flow was bubbled into the "SiO_2@="/H_2O dispersion for 1 h before 1.6 mL styrene and 48 mg BIS were added into the dispersion. After that, 20 mg potassium persulfate was added and then the system was vigorously stirred at 70 ^oC for 4 h. Subsequently, white powder was obtained by centrifugation. It was washed with absolute ethanol for several times before being vacuum-dried at 60 ^oC. The product was marked as SiO_2@PS in the following sections.

2.5 Preparation of SiO_2@sPS

First, N_2 flow was bubbled into 6 mL 1,2-dichloroethane for 0.5 h. Then, the 1,2-dichloroethane solvent was cooled in 10 wt% $CaCl_2$ ice bath under N_2 atmosphere. Third, 2 mL acetic anhydride was injected into the 1,2-dichloroethane solvent under vigorous stirring. 5 min later, 2.3 mL concentrated sulphuric acid was added into the solution. Just another 3 min later, this acetic anhydride/concentrated sulphuric acid/1,2-dichloroethane mixture was quickly injected into a N_2-pretreated homogeneous dispersion of 0.18 g SiO_2@PS and 10 mL 1,2-dichloroethane. The whole system was then vigorously stirred at 40 ^oC for 17 h under N_2 atmosphere. Subsequently, white powder was obtained by centrifugation. At last, it was washed with a mixture of absolute ethanol and cyclohexane (v:v = 1:1) for several times before being vacuum-dried at 70 ^oC. The product, sulfonated SiO_2@PS, was marked as SiO_2@sPS in the following sections.

2.6 Preparation of SiO_2@sPS+Nafion composite PEMs

SiO_2@sPS+Nafion composite PEMs were prepared by a blending-casting method. First, most solvent of the as-received Nafion solution was exchanged by DMF with the aid of rotary evaporation. Second, a desired amount of SiO_2@sPS nanoparticles were homogeneously dispersed in the Nafion/DMF solution by being sonicated for 1 h. The concentration of SiO_2@sPS was determined according to the weight of Nafion polymer. Third, the SiO_2@sPS/Nafion/DMF dispersion was carefully cast onto a rectangular mould in a vacuum oven under 70 ^oC. The temperature was gradually raised to 120 ^oC in 6 h. Then, the membrane was further dried under vacuum at 120 ^oC overnight. Fourth, the membrane was peeled off from the mould, followed by being treated in 3 wt% H_2O_2 solution at 70 ^oC for 2 h and then immersed in 1 M H_2SO_4 solution at 80 ^oC for another 1 h. At last, the membrane was rinsed by deionized H_2O for several times. The membrane thickness was controlled around 60 ± 10 μm. The composite PEM with 0.5 wt% (1.0 wt%, 2.0 wt%) loading of SiO_2@sPS was marked as 0.5 wt% (1.0 wt%, 2.0 wt%) SiO_2@sPS+Nafion in the following sections. Recast Nafion membrane was also prepared for comparison.[37]

2.7 Preparation of the 1.0 wt% h-sPS+Nafion composite PEM

The as-prepared 1 wt% SiO_2@sPS+Nafion composite PEM was immersed in excess 10 wt% HF solution under 30 ^oC for 24 h to completely dissolve SiO_2. Then, the membrane was immersed in 3 wt% H_2O_2 solution at 70 ^oC for 2 h and then boiled in 1 M H_2SO_4 solution at 80 ^oC for another 1 h to transform into the H^+ form. Lastly, the membrane, marked as 1.0 wt% h-sPS+Nafion, was rinsed by deionized H_2O for several times and stored in H_2O.

2.8 Characterizations of SiO_2, "SiO_2@=", SiO_2@PS, SiO_2@sPS and h-sPS

The morphology was observed with a field emission scanning electron microscopy (FE-SEM, Hitachi, S-4800). All the samples were coated by gold before the FE-SEM characterization. The transmission electron microscopy (TEM) images were obtained by a JEOL JEM2100 TEM instrument operated under an acceleration voltage of 200 eV. Fourier transform infrared spectroscopy (FTIR) was conducted on a Nicolet Nexus 470 spectrometer with a resolution of 4 cm^{-1} and 64 scans. Thermo gravimetric analyses (TGA) were performed under N_2 atmosphere with a Perkin Elmer Thermal Analyzer at a heating rate of 20 $^oC \cdot min^{-1}$. ^1H NMR (nuclear magnetic resonance) spectra were measured on a Varian Mercury plus 400 M spectrometer with D-DMSO as the solvent and tetramethylsilane as the internal reference.

2.9 Characterizations of PEMs

Attenuated total reflectance Fourier transform infrared spectroscopy (ATR-FTIR) was measured on a Nicolet Nexus 470 spectrometer with a resolution of 4 cm^{-1} and 64 scans. TGA analyses were conducted with a Perkin Elmer Thermal Analyzer at a heating rate of 10 $^oC \cdot min^{-1}$ under N_2 atmosphere. X-ray diffraction (XRD) was performed on a PANalytical X'pert diffractometer with Cu Kα radiation. Membrane morphology was observed by a scanning electron microscopy (SEM, XL 30 ESEM-TMP PHILIP). All the samples were coated with gold before the SEM observation. TEM was performed on a JEOL JEM2100 TEM instrument operated at a 200 eV acceleration voltage.

Water uptake (WU) was obtained as follows:[4] first, W_{dry} was measured after the membrane was dried at 80 ^oC for at least 24 h. Then, the membrane was fully hydrated by being immersed in H_2O at room temperature for 24 h. Subsequently, it was taken out and quickly sandwiched by two pieces of filter papers to completely remove the water on the membrane surfaces. Immediately, the membrane was enclosed in a sealed weighing bottle and weighted (W_{wet}). WU was estimated by the following equation: $WU(\%) = [(W_{wet} - W_{dry}) / W_{dry}] \cdot 100$.

Differential scanning calorimetry (DSC), carried out using Mettler-Toledo differential scanning calorimeter thermal analyzer in N_2 atmosphere, was employed to determine the contents of freezable (free) and non-freezable (bonded) water inside the membranes via melting transitions.[38] The tested samples, enclosed in aluminum pans, were first cooled from room temperature to -20 ^oC and then heated to 40 ^oC at a heating rate of 5 ^oC/min. The ratio of free water (R_f) to the H_2O-saturated PEM was estimated based on its melting enthalpy (ΔH_m) as follows: $R_f = \Delta H_m / H_m(ice)$ where $H_m(ice)$ refers to the heat of fusion of pure ice (334 J/g).[38] The content of bonded water was obtained by subtracting R_f from the WU value of corresponding PEM.

Proton conductivity was measured by a four-electrode method utilizing AC impedance spectroscopy between 0.1 MHz and 1 Hz with potentiostat control (CHI660d Model).[37] During the entire measurement, the tested conditions, i.e. humidity and

temperature, were controlled by a temperature-and-humidity test chamber. The investigated sample was equilibrated under the desired conditions for 8 h before the measurement.

Methanol permeability was measured with the aid of a home-made equipment under 25 and 50 °C (Fig. S1), and the digital photos of the whole set for methanol permeability measurement are presented in Fig. S2.[39] First, a dry PEM was put onto the ZnSe crystal of the ATR cell (Nicolet Nexus 470 FTIR spectrometer) and then sandwiched between the crystal and the PTFE mould (Fig. S1). Second, continuous ATR-FTIR data were acquired as soon as 0.5 mL of methanol/H_2O mixture (the volume ratio of methanol to H_2O is 4:1) was injected into the PTFE mould through a little hole (Fig. S1, Fig. S2 (E-F)). The little hole was blocked during the entire test to avoid any evaporation of methanol. The ATR-FTIR data, with a spectral resolution of 4 cm^{-1}, were taken as a function of diffusion time. The acquisition time interval is 40 s. Third, according to the increase in the peak area of -CH_3 stretching vibrations, the Fickian diffusion equation (eq 1), put forward by Fieldson and Barbari,[40] was applied to estimate the diffusion coefficients of methanol in the PEMs.[41]

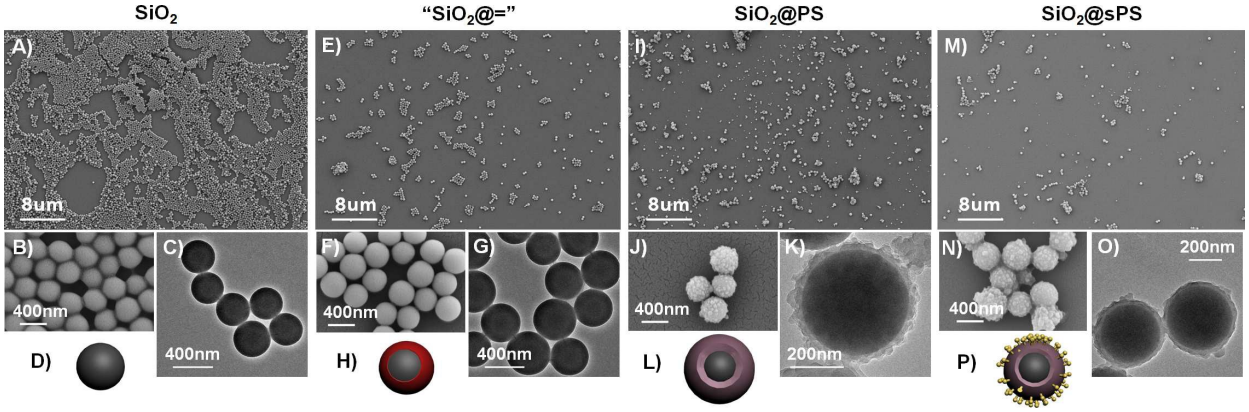

Fig. 1 FE-SEM images of SiO_2 (A-B), "SiO_2@=" (E-F), SiO_2@PS (I-J) and SiO_2@sPS (M-N); TEM images of SiO_2 (C), "SiO_2@=" (G), SiO_2@PS (K) and SiO_2@sPS (O); schematic illustration of SiO_2 (D), "SiO_2@=" (H), SiO_2@PS (L) and SiO_2@sPS (P).

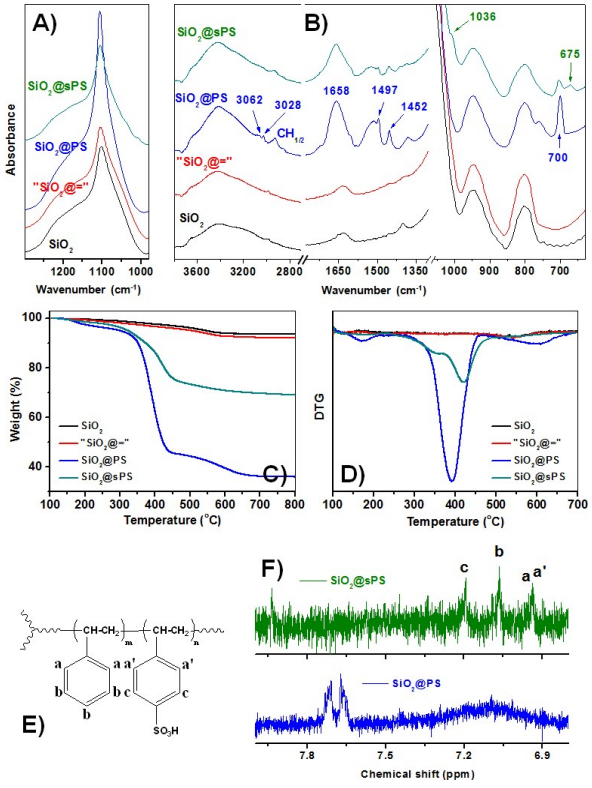

Fig. 2 FTIR spectra (A-B) and TGA analyses (C-D) of SiO_2, "SiO_2@=", SiO_2@PS and SiO_2@sPS; (E) chemical structure of the sPS shell; (F) ^1H NMR spectra of SiO_2@PS and SiO_2@sPS.

3 Results and Discussion

3.1 Characterizations of SiO_2, "SiO_2@=", SiO_2@PS and SiO_2@sPS

Fig. 1 depicts the morphologies of SiO_2, "SiO_2@=", SiO_2@PS and SiO_2@sPS by SEM and TEM techniques. SiO_2 presents an excellent spherical structure with a diameter of 330 nm and mono-disperses in size (Fig. 1 (A-D)). As its FTIR spectrum shown in Fig. 2 (A), SiO_2 possesses the typical IR absorption of the stretching vibration of Si-O-Si linkages at 1101 cm^{-1}. With respect to"SiO_2@=", no obvious FTIR peak typical of C=C groups is detected in its FTIR spectrum probably because the amount of the C=C precursor MPS modified onto the SiO_2 surface is quite low (Fig. 2 (B)). Based on the TGA analyses (Fig. 2 (C)), compared to SiO_2, "SiO_2@=" presents a slightly larger weight loss (about 1.6 wt%) at 800 °C because of the decomposition of alkyl chains derived from MPS. Actually, only a small quantity of C=C groups, affording to subsequently graft PS chains onto the surface of SiO_2, is necessary. Hence, no big morphology difference is found between SiO_2 and "SiO_2@=" based on their SEM and TEM images (Fig. 1 (A-G)), and only a slight increase in the particle size is observed in "SiO_2@=" due to the modification of MPS. For SiO_2@PS, a rough polymer layer with an average thickness of about 38 nm has formed on the surface of SiO_2 (Fig. 1 (I-L)). Distinctive IR absorptions of PS chains are detected in its FTIR spectrum (Fig. 2 (B)). The IR peaks at 3062 and 3028 cm^{-1} are attributed to the stretching vibrations of the C-H groups belonging to the benzene rings, while the bending vibrations of these C-H groups correspond to the sharp IR peak at 700 cm^{-1}.[42] The benzene rings themselves present three typical IR absorptions at 1452, 1497 and 1658 cm^{-1},

respectively. Besides, the IR peaks stemmed from the stretching vibrations of the $CH_{(1/2)}$ groups in PS backbones, below 3000 cm^{-1}, can be also observed in the FTIR spectrum of SiO_2@PS (Fig. 2 (B)). TGA analysis reveals that about 56 wt% PS is attached onto the surface of SiO_2 (Fig. 2 (C)).

However, after the sulfonation modification, only 23 wt% sPS with a uniform layer thickness of about 25 nm (Fig. 1 (M-P)) remains on the surface of SiO_2 (Fig. 2 (C)). It is because that the loosely attached i.e. un-crosslinked PS chains have been removed during the sulfonation process. Compared to that of SiO_2@PS, the decomposition temperature of the PS shell of SiO_2@sPS shifts from 392 up to 421 °C (Fig. 2 (D)). It is worth noting that the DTG peak around 350 °C corresponds to the desulfonation process of SiO_2@sPS (Fig. 2 (D)). The FTIR spectrum of SiO_2@sPS also confirms the successful sulfonation modification by displaying two IR peaks at 1036 and 675 cm^{-1}, respectively corresponding to the stretching vibrations of $–SO_3H$ and C-S groups (Fig. 2 (B)).[43] The degree of sulfonation (DS) of SiO_2@sPS is addressed with the aid of ^1H NMR technique. Fig. 2 (E) proposes the chemical structure of the sPS shell, and Fig. 2 (F) presents the ^1H NMR spectra of SiO_2@PS and SiO_2@sPS. For SiO_2@PS, the two ^1H NMR peaks between 7.6 and 7.8 ppm are attributed to the H atoms belonging to the benzene rings of PS, while the detailed assignment of the ^1H NMR peaks of SiO_2@sPS is provided in Fig. 2 (E/F). Thereby, DS is estimated as $DS(\%) = 100\% * (c/2)/[(c/2) + (b/3)]$, where b and c refer to the areas of the ^1H NMR peaks labelled as "b" and "c" in Fig. 2 (F), respectively.[44] Herein, the DS value of SiO_2@sPS is estimated to be about 57 % of PS repeated units.

3.2 Characterizations of SiO_2@sPS+Nafion composite PEMs

Generally, the hydrophobic backbones $(-CF_2-)_n$ and hydrophilic $–SO_3H$ groups of Nafion present their symmetric stretching vibrations at 1151 and 1055 cm^{-1}, respectively, while their asymmetric stretching vibrations display a superimposed IR peak at 1213 cm^{-1} (Fig. 3 (A)). The doublet around 982 and 970 cm^{-1}, also typical for Nafion polymer, corresponds to the stretching vibrations of the -COC- linkages in its side chains.[4] When SiO_2@sPS was incorporated into the Nafion matrix, the IR peaks at both 1213 and 1151 cm^{-1} shift evidently in the FTIR spectra of 0.5, 1 and 2 wt% SiO_2@sPS+Nafion membranes. It demonstrates the existence of strong interactions between SiO_2@sPS and the Nafion matrix. Such interactions probably come from 1) the hydrogen bonding interactions between $–SO_3H$ (SiO_2@sPS) --- $–SO_3H$ (Nafion)[45] and 2) the hydrophobic interactions between PS chains and Nafion backbones.[46] Meanwhile, the IR absorption at 1055 cm^{-1} was strengthened because of the introduction of more $-SO_3H$ groups into the membrane matrix. Understandably, with the SiO_2@sPS concentration increasing from 0 wt% to 2.0 wt%, the shoulder peak around 1100 cm^{-1}, assigned to the stretching vibrations of Si-O-Si linkages, becomes more evident. And a similar trend is also observed on the stretching vibrations of the $CH_{(1/2)}$ groups of PS at about 3062 and 3028 cm^{-1}.

XRD is a powerful technique to make affirmations about the microstructure changes of Nafion-based PEMs.[47,48] A very broad peak is usually observed in the XRD pattern of Nafion membrane around 2θ=17° (Fig. 3 (B)). To put it more specific, the amorphous regions of Nafion membrane mainly contribute to the lower-2θ part (about 16.1°) of its XRD peak around 2θ=17°, while the higher-2θ part (about 17.7°) is attributed to its crystalline regions.[47,48] Compared to that of the recast Nafion, the peak around 2θ=17° shifts slightly to lower 2θ in the XRD patterns of SiO_2@sPS+Nafion membranes, and the shift degree seems to be proportional to the SiO_2@sPS concentration. It indicates that the strong interactions between SiO_2@sPS and Nafion matrix somewhat hinder the crystallization of Nafion membrane. The TGA analyses in Fig. 3 (C/D) also reveal the existence of interactions between SiO_2@sPS and the Nafion matrix. A very slight increase in the decomposition temperatures of Nafion backbones and side chains can be obtained in SiO_2@sPS+Nafion probably due to strong interactions between SiO_2@sPS and Nafion. Many prior studies also found that the strong interactions between the incorporated additives and Nafion backbones could effectively enhance the thermal stability of Nafion backbones.[4,46] Such interactions probably retard the decomposition reactions of Nafion backbones. To some extent, SiO_2@sPS suppressing the diffusion of decomposed products during the heating process may also make a contribution to this phenomenon.[4]

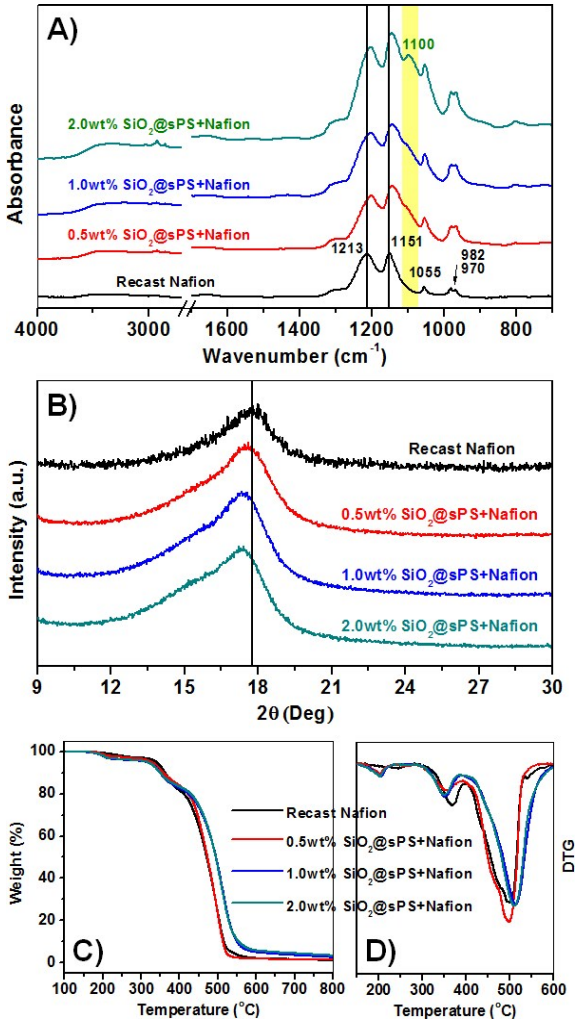

Fig. 3 ATR-FTIR spectra (A), XRD patters (B) and TGA analyses (C-D) of the recast Nafion and SiO_2@sPS+Nafion membranes.

The intensity of the XRD peak is actually in proportion to the electron density difference between the ionic cluster domains and the backbone regions of Nafion membrane.[46,47] As depicted in Fig. 3 (B), the peak intensity increases in the SiO_2@sPS+Nafion membranes because of the introduction of more -SO_3H groups into membrane matrix. These additional -SO_3H groups can interact with the original -SO_3H groups of Nafion polymer via hydrogen bonding interactions. It enlarges the size of ionic clusters and then increases the electron density difference between the ionic cluster domains and the backbone regions. This is also the reason that the desulfonation process shifts obviously toward lower temperature in the SiO_2@sPS+Nafion membranes (Fig. 3 (D)).[39,46] Hong discovers that larger ionic cluster possesses relatively lower desulfonation temperature,[46] which is also confirmed by our own previous experimental results.[4,37]

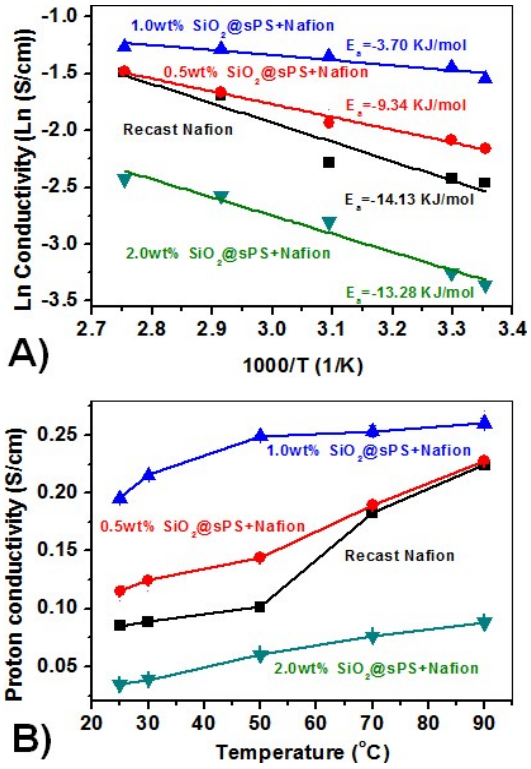

Fig. 4 Temperature-dependent proton conductivities (A) and Arrhenius plots (B) of the recast Nafion and SiO_2@sPS+Nafion membranes under 100% RH.

The enlarged ionic clusters and hence optimized ionic channels intensively benefit the proton transport in the 0.5 wt% and 1.0 wt% SiO_2@sPS+Nafion membranes, as the activation energies of proton conduction illustrated in Fig. 4 (A). The activation energy of recast Nafion is about 14.13 KJ/mol under 100% RH, while those of the 0.5 wt% and 1.0 wt% SiO_2@sPS+Nafion membranes decrease down to 8.34 KJ/mol and 3.70 KJ/mol, respectively. Thereby, the 0.5 wt% and 1.0 wt% SiO_2@sPS+Nafion membranes present greatly enhanced proton conductivity compared to the recast Nafion membrane (Fig. 4 (B)). While with regard to the 2.0 wt% SiO_2@sPS+Nafion membrane, it shows a decrease rather than an increase in the proton conductivity compared to the recast Nafion, probably resulting from the aggregation of SiO_2@sPS nanoparticles.

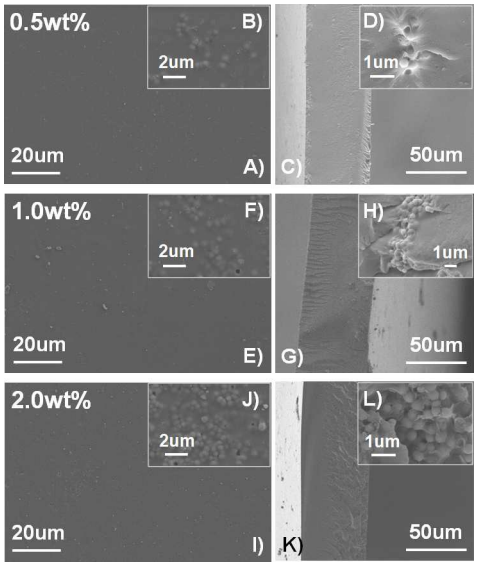

Fig. 5 Surface SEM images of the 0.5 (A-B), 1.0 (E-F) and 2.0 wt% (I-J) SiO_2@sPS+Nafion membranes; cross-sectional SEM images of the 0.5 (C-D), 1.0 (G-H) and 2.0 wt% (K-L) SiO_2@sPS+Nafion membranes.

Table 1 Methanol permeability of the recast Nafion, 0.5, 1.0, 2.0 wt% SiO_2@sPS+Nafion and 1.0 wt% h-sPS+Nafion membranes under 80v/v% methanol/H_2O (the volume ratio of methanol to H_2O is 4:1).

PEMs	Methanol permeability (P, $*10^{-8}$ cm^2/s) 25 °C		50 °C	
recast Nafion	37.76	±2.08	/[a]	/[a]
0.5 wt% SiO_2@sPS+Nafion	12.07	±0.27	21.17	±2.88
1.0 wt% SiO_2@sPS+Nafion	8.99	±0.15	40.71	±2.05
2.0 wt% SiO_2@sPS+Nafion	6.92	±0.81	26.24	±1.54
1.0 wt% h-sPS+Nafion	2.31	±0.27	6.19	±0.24

[a]The methanol crossover of the recast Nafion membrane is extremely extensive at 50 °C under 80v/v% methanol/H_2O. Under this circumstance, the methanol permeability cannot be properly measured by the equipment shown in Fig. S1/2.

The as-prepared composite PEMs are all transparent, as their digital photos shown in Fig. S3. The strong interactions between SiO_2@sPS and Nafion matrix bestow good dispersion upon SiO_2@sPS in the Nafion matrix when the SiO_2@sPS concentration stays below 1.0 wt%, as demonstrated by the SEM images in Fig. 5. When its concentration increases to 2.0 wt%, some large aggregations of SiO_2@sPS have emerged in the membrane (Fig. 5 (J/L)). It may disrupt the typical hydrophobic/hydrophilic micro-phase separation of Nafion membrane which is the guarantee of its good transport properties.[46,49] Further increasing the incorporated concentration of SiO_2@sPS is improper and may be bad for the membrane performance.

With respect to another crucial transport property of Nafion membranes, i.e. methanol crossover, SiO_2@sPS can increase the tunnel zigzag of diffusion pathways for bulk methanol, leading to the formation of obstructed channels against methanol crossover. Therefore, compared to the recast Nafion membrane, the SiO_2@sPS+Nafion membranes possess lower methanol permeability under both 25 and 50 °C, as shown in Table 1. Therefore, the SiO_2@sPS+Nafion membranes present significantly enhanced membrane selectivity.

3.3 Characterizations of the 1 wt% h-sPS+Nafion composite PEM

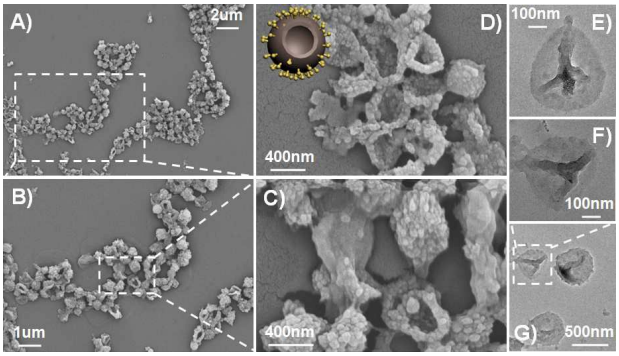

Fig. 6 SEM (A-D) and TEM images (E-G) of the h-sPS spheres.

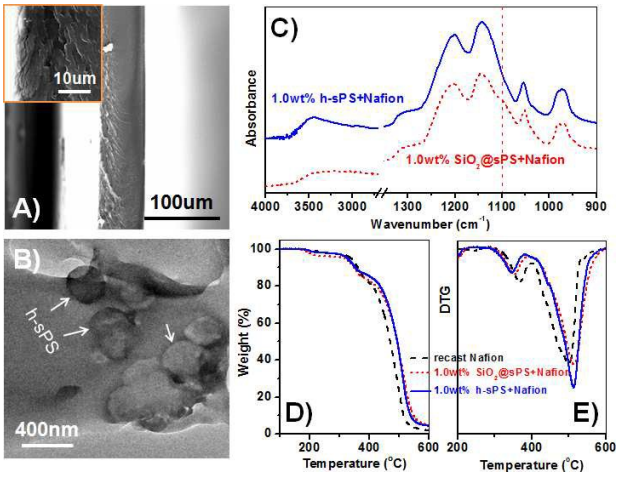

Fig. 7 Cross-sectional SEM images (A), cross-sectional TEM image (B), FTIR spectrum (C) and TGA analyses (D-E) of the 1.0 wt% h-sPS+Nafion membrane; The FTIR and TGA data of the recast Nafion and 1.0 wt% SiO_2@sPS+Nafion membranes are also provided for comparison.

Further enhancement of membrane performance is explored by creating well-dispersed nano-sized hollow spheres inside the membrane matrix via a template etching method. Considering that the 1.0 wt% SiO_2@sPS+Nafion membrane possesses relatively higher proton conductivity, we select it as the subject investigated in this section to strengthen the distinctive advantages of our approach. Herein, membrane porosity is achieved by HF solution etching of the acid labile SiO_2 core leaving the chemically stable sPS shell intact. As indicated by the SEM and TEM images (Fig. 6), the spherical hollow structure of h-sPS retains pristine when the SiO_2 core is removed, and its lumen size is similar to the size of the SiO_2 core. Fig. 7 (A/B) shows the cross-sectional SEM and TEM images of the 1.0 wt% h-sPS+Nafion membrane. Obviously, no SiO_2@sPS nano-particle is observed now, confirming the successful removal of the SiO_2 core from the composite PEM. It parallels the finding in Fig. 7 (C) that the peak at 1100 cm^{-1}, typical for the stretching vibrations of Si-O-Si linkages, disappears in the FTIR spectrum of the 1.0 wt% h-sPS+Nafion membrane. Resultantly, well dispersed h-sPS spheres remains with the generation of nano-sized uniform hollow structures inside the membrane matrix. Such an etching process does not negatively affect the strong interactions between sPS and the Nafion matrix, because increased decomposition temperature of Nafion backbones is still found in the 1.0 wt% h-sPS+Nafion membrane (Fig. 7 (D-E)).

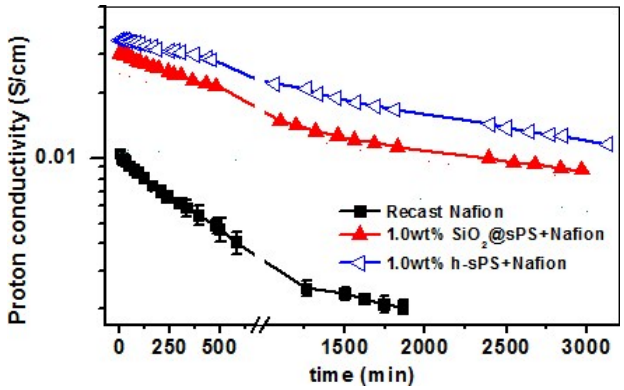

Fig. 8 Time-dependent proton conductivities of the recast Nafion, 1.0 wt% SiO_2@sPS+Nafion and 1.0 wt% h-sPS+Nafion membranes under 40% RH at 100 °C.

These new-formed hollow spheres, acting as the similar role of vacuoles in plant cells, would hold more water inside the membrane matrix and hence slow down the rate of water loss of Nafion membrane under higher-temperature and low-humidity conditions. In other words, the 1.0 wt% h-sPS+Nafion membrane has stronger water retention capability. Fig. 8 presents the time-dependent proton conductivities of the recast Nafion, 1.0 wt% SiO_2@sPS+Nafion and 1.0 wt% h-sPS+Nafion membranes under 40% RH at 100°C. Recast Nafion losses its proton conductivity very quickly. About 60% of its proton conductivity vanishes at t=580 min, and the lost proton conductivity reaches up to 80% of its original value at t=1860 min. It is a result of the typical drawback of Nafion membrane that it losses H_2O very fast under higher-temperature and low-humidity conditions. With regard to the 1.0 wt% SiO_2@sPS+Nafion membrane, its proton conductivity is more stable during the entire test. About 70% loss of its proton conductivity is found when the dehydration time reaches almost 3000 min. Its enlarged ionic clusters and optimized ionic channels facilitate the proton transport in the 1.0 wt% SiO_2@sPS+Nafion membrane.

Generally, proton transport through PEM obeys Grotthuss mechanism ("hopping" mechanism) and vehicle mechanism. The former refers to the proton hopping from one proton donator to a neighboring proton acceptor via hydrogen bonds, which is directly related to the interconnection condition of ionic cluster

channels inside the PEM matrix. The latter refers to the diffusion of protonated water molecules, such as H_3O^+ and $H_5O_2^+$, where high water retention capability of the PEM plays an indispensible role. Further enhancement of proton conductivity is obtained in the 1.0 wt% h-sPS+Nafion membrane. The 1.0 wt% h-sPS+Nafion membrane not only inherits the advantages of the 1.0 wt% SiO_2@sPS+Nafion membrane, but also is able to hold more water inside the h-sPS spheres,[3,35,36] which is beneficial for the proton transfer via both Grotthuss mechanism and vehicle mechanism. This consideration is demonstrated by the WU measurement shown in Table 2. The 1.0 wt% SiO_2@sPS+Nafion membrane possesses a higher WU value compared to recast Nafion due to the hydrophilicity of SiO_2@sPS, and the 1 wt% h-sPS+Nafion membrane presents a further increase in WU owing to the hollow structure of h-sPS spheres.

Table 2. Water uptake values, fractions of free water and bonded water of the recast Nafion, 1.0 wt% SiO_2@sPS+Nafion and 1.0 wt% h-sPS+Nafion membranes.

PEMs	WU (%)	Free water (%)	Bonded water (%)
Recast Nafion	20.51	7.83	12.68
1.0 wt% SiO_2@sPS+Nafion	24.39	7.63	16.76
1.0 wt% h-sPS+Nafion	29.03	11.96	17.07

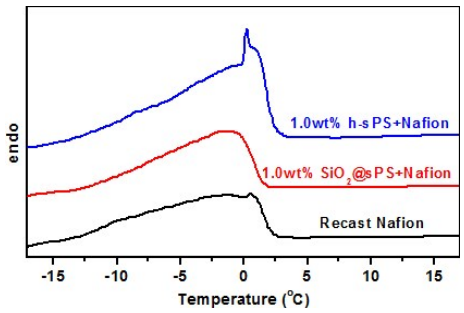

Fig. 9 DSC curves of fully hydrated recast Nafion, 1.0 wt% SiO_2@sPS+Nafion and 1.0 wt% h-sPS+Nafion membranes at a heating rate of 5 °C/min.

Detailed information of water state, i.e. the fraction of free water or freezable water that does not interact with $-SO_3H$ groups, and the fraction of bonded water or non-freezable water, is revealed by DSC analyses (Fig. 9 and Table 2). The 1.0 wt% SiO_2@sPS+Nafion membrane has a comparable fraction of free water with recast Nafion, and its enhanced water retention capability mainly lies in the increased amount of bonded water interacting with the additional of $-SO_3H$ groups. The increased amount of bonded water ensures continuous water networks, imparting higher proton conductivity under higher-temperature and low-humidity conditions (Fig. 8).[38] For the 1.0 wt% h-sPS+Nafion membrane, the fractions of both of these two types of water increases. H_2O-filled h-sPS spheres, acting as water reservoirs, can hydrate the membrane in turn by releasing H_2O gradually, which guarantees the high proton conductivity of the 1.0 wt% h-sPS+Nafion membrane under high-temperature and low-humidity conditions. With respect to the Nafion-based PEMs modified by various other sulfonated materials, optimized proton conductivity is usually observed under high-humidity and moderate-temperature conditions (Fig. 10, Table S1). While for the 1.0 wt% h-sPS+Nafion membrane, its performance enhancement is very evident (Fig. 10, Table S1). Especially under severe conditions, hollow sphere structure further strengthens this distinctive advantage, hence an increase in proton conductivity even by orders of magnitude is found. Probably, the strong interactions between h-sPS and the ionic clusters of Nafion benefit the effective use of H_2O released by h-sPS to contribute to the high proton conductivity. Besides, in terms of proton conductivity under relatively high humidity, the 1.0 wt% SiO_2@sPS+Nafion membrane also presents obvious advantages over the other Nafion-based PEMs modified by optimized sulfonated materials with optimized incorporation content (Fig. 10, Table S1).

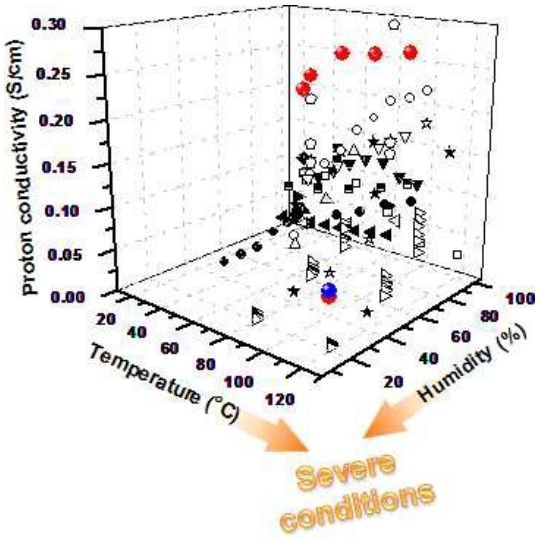

Fig. 10 Proton conductivity comparison between the 1.0 wt% SiO_2@sPS+Nafion (red), 1.0 wt% h-sPS+Nafion (blue) membranes and various Nafion-based PEMs modified by other sulfonated materials (black)[6,7,17,18,21,23-30,33,50-53].

Besides, h-sPS can further suppress the penetration of methanol by blocking it inside the hollow spheres.[35,36] As shown in Table 1, the 1.0 wt% h-sPS+Nafion membrane presents a much lower methanol permeability compared with the 1.0 wt% SiO_2@sPS+Nafion one. A schematic illustration is provided in Fig. 11. Herein, a "H_2O donating/methanol accepting" mechanism is proposed to explain the further enhancement of the membrane performance of h-sPS+Nafion. It provides another promising approach to alleviate critical disadvantages of Nafion membranes and hence prepare high-performance Nafion-based PEMs.

4 Conclusions

Imbedding SiO_2@sPS nanoparticles into Nafion matrix can effectively increase the selectivity of the as-prepared SiO_2@sPS+Nafion composite PEMs. First, the additional $-SO_3H$ groups enlarge the ionic clusters and hence benefit the proton conduction. The SiO_2@sPS+Nafion membrane has a larger amount of bonded water, ensuring continuous water networks and hence contributing to its high proton conductivity. Second,

SiO_2@sPS increases the tunnel zigzag of the diffusion pathways for bulk methanol, enhancing the methanol resistance of the SiO_2@sPS+Nafion membrane.

Besides, etching the SiO_2 core leads to the formation of well-dispersed uniform hollow spheres inside the membrane matrix. The intact h-sPS spheres can reserve more free water which is gradually released to hydrate the membrane in turn under high-temperature and low-humidity conditions. Therefore, a further increase in the proton conductivity of the h-sPS+Nafion membrane is found. Moreover, by blocking methanol inside the h-sPS spheres, its methanol resistance is further enhanced. Herein, a "H_2O donating/methanol accepting" platform is first proposed. It may provide another promising approach to alleviate critical disadvantages of Nafion membranes and hence prepare highly selective PEMs.

Acknowledgements

The authors are very grateful for the financial support of the National Natural Science Foundation of China (NSFC) (No. 21276051), Chinese doctoral fund (20110071130001) and the National Basic Research Program of China (2009CB930000).

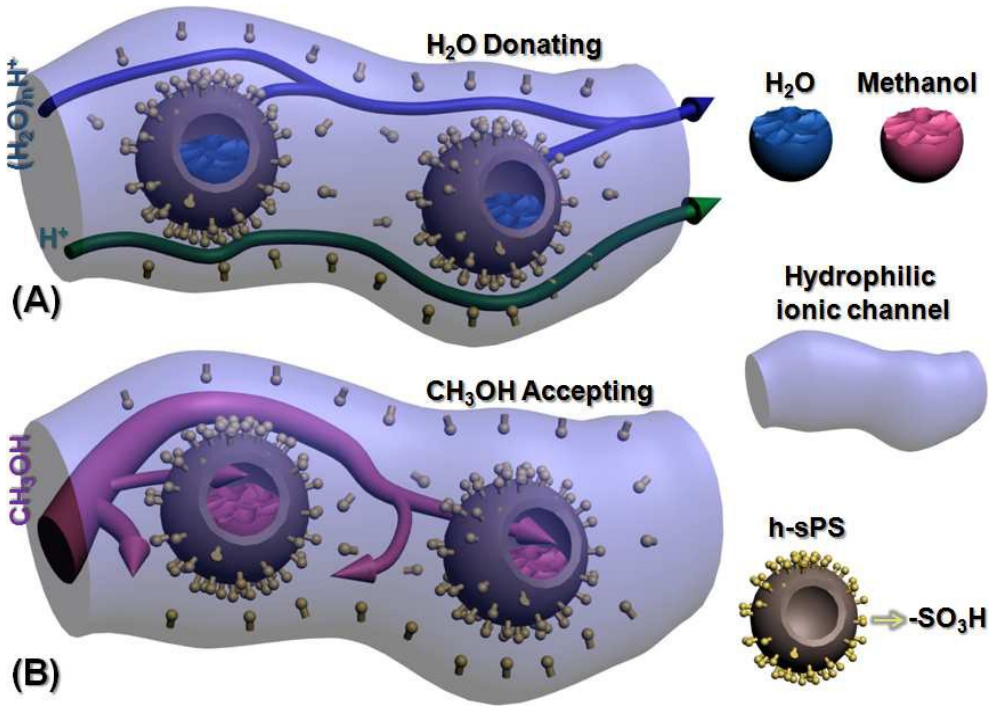

Fig. 11 Schematic illustration of the proposed "H_2O donating/methanol accepting" mechanism.

Notes and references

State Key Laboratory of Molecular Engineering of Polymers, Collaborative Innovation Center of Polymers and Polymer Composite Materials, Department of Macromolecular Science, Laboratory of Advanced Materials, Fudan University, Shanghai, 200433, P. R. China. E-mail: bbtang@fudan.edu.cn , or *peiyiwu@fudan.edu.cn.*

† Electronic Supplementary Information (ESI) available: Schematic illustration of the home-made equipment used to characterize the methanol permeability of PEMs (Fig. S1); Digital photos of the whole set used to characterize the methanol permeability of PEMs (Fig. S2); Digital photos of the recast Nafion, 0.5~2.0 wt% SiO_2@sPS+Nafion and 1.0 wt% h-sPS+Nafion membranes (Fig. S3); Detailed information about the optimized proton conductivity of Nafion-based PEMs modified by various other sulfonated materials (Table S1). See DOI: 10.1039/b000000x/.

1 M. M. Nasef, *Chem. Rev.*, 2014, **114**, 12278-12329.
2 H. W. Zhang and P. K. Shen, *Chem. Rev.*, 2012, **112**, 2780-2832.
3 J. T. Wang, X. J. Yue, Z. Z. Zhang, Z. Yang, Y. F. Li, H. Zhang, X. L. Yang, H. Wu and Z. Y. Jiang, *Adv. Funct. Mater.*, 2012, **22**, 4539-4546.
4 K. Feng, B. B. Tang and P. Y. Wu, *J. Mater. Chem. A*, 2014, **2**, 16083-16092.
5 H. Kim, M. S. Kang, D. H. Lee, J. Won, J. Kim and Y. S. Kang, *J. Membr. Sci.*, 2007, **304**, 60-64.
6 J. D. Jeon and S. Y. Kwak, *J. Power Sources*, 2008, **185**, 49-54.
7 B. Bae, H. Y. Ha and D. Kim, *J. Membr. Sci.*, 2006, **276**, 51-58.
8 Y. Z. Fu, A. Manthiram and M. D. Guiver, *Electrochem. Commun.*, 2006, **8**, 1386-1390.
9 Y. Z. Fu, A. Manthiram and M. D. Guiver, *Electrochem. Commun.*, 2007, **9**, 905-910.
10 F. Wang, M. Hickner, Y. S. Kim, T. A. Zawodzinski and J. E. McGrath, *J. Membr. Sci.*, 2002, **197**, 231-242.
11 L. Sha Wang, A. Nan Lai, C. Xiao Lin, Q. Gen Zhang, A. Mei Zhu and Q. Lin Liu, *J. Membr. Sci.*, 2015, **492**, 58-66.
12 T. Mochizuki, M. Uchida, H. Uchida, M. Watanabe and K. Miyatake, *ACS Appl. Mater. Interfaces*, 2014, **6**, 13894-13899.
13 M. M. Hasani-Sadrabadi, E. Dashtimoghadam, F. S. Majedi, S. H. Emami and H. Moaddel, *Int. J. Hydrogen Energy*, 2011, **36**, 6105-6111.
14 S. Mondal, S. Soam and P. P. Kundu, *J. Membr. Sci.*, 2015, **474**, 140-147.
15 K. Y. Cho, H. Y. Jung, K. A. Sung, W. K. Kim, S. J. Sung, J. K. Park, J. H. Choi and Y. E. Sung, *J. Power Sources*, 2006, **159**, 524-528.
16 H. J. Kim, H. J. Kim, Y. G. Shul and H. S. Han, *J. Power Sources*, 2004, **135**, 66-71.
17 R. Kannan, M. Parthasarathy, S. U. Maraveedu, S. Kurungot and V. K. Pillai, *Langmuir*, 2009, **25**, 8299-8305.
18 Y. Jun, H. Zarrin, M. Fowler and Z. Chen, *Int. J. Hydrogen Energy*, 2011, **36**, 6073-6081.
19 H. Zarrin, D. Higgins, Y. Jun, Z. W. Chen and M. Fowler, *J. Phys. Chem. C*, 2011, **115**, 20774-20781.

20 F. Pereira, K. Vallé, P. Belleville, A. Morin, S. Lambert and C. Sanchez, *Chem. Mater.*, 2008, **20**, 1710-1718.

21 Y. Tominaga, I. C. Hong, S. Asai and M. Sumita, *J. Power Sources*, 2007, **171**, 530-534.

22 Y.-F. Lin, C.-Y. Yen, C.-C. M. Ma, S.-H. Liao, C.-H. Lee, Y.-H. Hsiao and H.-P. Lin, *J. Power Sources*, 2007, **171**, 388-395.

23 C. H. Tsai, H. J. Lin, H. M. Tsai, J. T. Hwang, S. M. Chang and Y. W. Chen-Yang, *Int. J. Hydrogen Energy*, 2011, **36**, 9831-9841.

24 C. M. Wang, E. Chalkova, J. K. Lee, M. V. Fedkin, S. Komarneni and S. N. Lvov, *J. Electrochem. Soc.*, 2011, **158**, B690-B697.

25 K. Fatyeyeva, C. Chappey, F. Poncin-Epaillard, D. Langevin, J.-M. Valleton and S. Marais, *J. Membr. Sci.*, 2011, **369**, 155-166.

26 P. Bébin, M. Caravanier and H. Galiano, *J. Membr. Sci.*, 2006, **278**, 35-42.

27 Y. Kim, Y. Choi, H. K. Kim and J. S. Lee, *J. Power Sources*, 2010, **195**, 4653-4659.

28 B. A. Holmberg, X. Wang and Y. Yan, *J. Membr. Sci.*, 2008, **320**, 86-92.

29 S. Meenakshi, A. K. Sahu, S. D. Bhat, P. Sridhar, S. Pitchumani and A. K. Shukla, *Electrochim. Acta*, 2013, **89**, 35-44.

30 H. Y. Li, Y. Y. Lee, J. Y. Lai and Y. L. Liu, *J. Membr. Sci.*, 2014, **466**, 238-245.

31 Y. F. Yao, L. W. Ji, Z. Lin, Y. Li, M. Alcoutlabi, H. Hamouda and X. W. Zhang, *ACS Appl. Mater. Interfaces*, 2011, **3**, 3732-3737.

32 J.-D. Jeon and S.-Y. Kwak, *J. Power Sources*, 2008, **185**, 49-54.

33 Y.-F. Lin, Y.-H. Hsiao, C.-Y. Yen, C.-L. Chiang, C.-H. Lee, C.-C. Huang and C.-C. M. Ma, *J. Power Sources*, 2007, **172**, 570-577.

34 W. Jia, K. Feng, B. Tang and p. wu, *J. Mater. Chem. A*, 2015, DOI: 10.1039/C5TA03381K

35 K. Ahn, M. Kim, K. Kim, H. Ju, I. Oh and J. Kim, *J. Power Sources*, 2015, **276**, 309-319.

36 W. Zhang, B. Zhang, G. W. He, B. Liu, Z. Y. Jiang, X. L. Yang and C. X. Li, *RSC Adv.*, 2015, **5**, 5343-5356.

37 K. Feng, B. B. Tang and P. Y. Wu, *ACS Appl. Mater. Interfaces*, 2013, **5**, 1481-1488.

38 M. M. Hasani-Sadrabadi, E. Dashtimoghadam, R. Nasseri, A. Karkhaneh, F. S. Majedi, N. Mokarram, P. Renaud and K. I. Jacob, *J. Mater. Chem. A*, 2014, **2**, 11334-11340.

39 K. Feng, B. B. Tang and P. Y. Wu, *ACS Appl. Mater. Interfaces*, 2013, **5**, 13042-13049.

40 G. T. Fieldson and T. A. Barbari, *Polymer*, 1993, **34**, 1146-1153.

41 H. J. Lai, Z. W. Wang, P. Y. Wu, B. I. Chaudhary, S. S. Sengupta, J. M. Cogen and B. Li, *Ind. Eng. Chem. Res.*, 2012, **51**, 9365-9375.

42 C. Y. Huang and C. L. Chen, *Surf. Coat. Technol.*, 2002, **153**, 194-202.

43 Y. F. Lin, Y. H. Hsiao, C. Y. Yen, C. L. Chiang, C. H. Lee, C. C. Huang and C. C. M. Ma, *J. Power Sources*, 2007, **172**, 570-577.

44 A. C. C. Yang, R. Narimani, Z. B. Zhang, B. J. Frisken and S. Holdcroft, *Chem. Mater.*, 2013, **25**, 1935-1946.

45 B. M. Gallant, X. W. Gu, D. Z. Chen, J. R. Greer and N. S. Lewis, *ACS Nano*, 2015, **9**, 5143-5153.

46 B. G. Choi, Y. S. Huh, Y. C. Park, D. H. Jung, W. H. Hong and H. Park, *Carbon*, 2012, **50**, 5395-5402.

47 K. Feng, L. Hou, B. B. Tang and P. Y. Wu, *Phys. Chem. Chem. Phys.*, 2015, **17**, 9106-9115.

48 M. Fujimura, T. Hashimoto and H. Kawai, *Macromolecules*, 1981, **14**, 1309-1315.

49 J. H. Kim, S. K. Kim, K. Nam and D. W. Kim, *J. Membr. Sci.*, 2012, **415**, 696-701.

50 Y. Kim, J. S. Lee, C. H. Rhee, H. K. Kim and H. Chang, *J. Power Sources*, 2006, **162**, 180-185.

51 K. Xu, C. Chanthad, M. R. Gadinski, M. A. Hickner and Q. Wang, *ACS Appl. Mater. Interfaces*, 2009, **1**, 2573-2579.

52 G. Gnana Kumar, A. R. Kim, K. Suk Nahm and R. Elizabeth, *Int. J. Hydrogen Energy*, 2009, **34**, 9788-9794.

53 Y. Choi, Y. Kim, H. K. Kim and J. S. Lee, *J. Membr. Sci.*, 2010, **357**, 199-205.

For Graphic Abstract

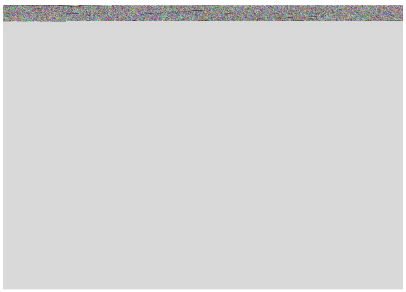

A "H_2O donating/methanol accepting" approach is exploited to alleviate critical drawbacks of Nafion and thereby fabricate highly selective PEMs.